J. Fluid Mech. (2011), *vol.* 686, *pp.* 583–606. © Cambridge University Press 2011
doi:10.1017/jfm.2011.352

Shock trains on a planar beach

Matteo Antuono†

CNR-INSEAN (The Italian Ship Model Basin), Via di Vallerano 139, 00128 Rome, Italy

(Received 15 November 2010; revised 13 June 2011; accepted 17 August 2011;
first published online 30 September 2011)

Following on from the author's previous work, the propagation of trains of shock waves on a planar beach is studied in the framework of the nonlinear shallow water equations. The analysis is based on the use of a quasi-analytical solution valid for a shock wave which is fed by a constant Riemann invariant. The asymptotic behaviour of a train of such shock waves is inspected and novel approximate analytical solutions are provided. These are useful both for representing fundamental physical scenarios (e.g. propagation of saw-tooth spilling breakers in the surf zone) and for benchmarking wave-resolving and wave-averaged theoretical/numerical solutions. Finally, a study of the energy dissipation induced by the shock train is provided.

Key words: surface gravity waves, wave breaking, waves/free-surface flows

1. Introduction

The study of wave breaking on beaches has always represented a topic of great interest for the coastal scientific community. Apart from the intrinsic fascinating aspects of breaking events, a wide range of physical phenomena are related to wave breaking and are of crucial importance for the coast evolution and protection. Just to cite a few of these, breaking events are the main cause of sediment mobilization/transport and coastal erosion on sandy beaches (Elfrink & Baldock 2002; Pritchard & Hogg 2005) and, further, they represent a forcing term for rip and longshore currents (Brocchini *et al.* 2004; Kennedy *et al.* 2006; Guard & Baldock 2007; Brocchini & Dodd 2008; Zhang & Liu 2008).

Over the years, several numerical schemes have been developed to model the surf zone flows. The most famous and widespread in the coastal community are all based on depth averages of the local flow equations (e.g. the Navier–Stokes equations or the Laplace equation) over the water depth. These models are the nonlinear shallow water equations (NSWEs; see, for example, Park & Borthwich 2001; Brocchini *et al.* 2001; Hubbard & Dodd 2002) and the numerous Boussinesq-type models (e.g. Kennedy *et al.* 2000; Briganti *et al.* 2004). Averaging these models over the wave period leads to the definition of the so-called wave-averaged models (Van Dongeren *et al.* 1994; Booij, Ris & Holthuijsen 1999) which are widely used to model longer-time events (such as, for example, wave currents). With respect to the latter ones, the NSWEs and the Boussinesq-type models are usually called 'wave-resolving' models.

The NSWEs are surely the simplest and most suited equations for the modelling of wave breaking since, due to their hyperbolic structure, they allow for a simple and

† Email address for correspondence: matteoantuono@gmail.com

https://doi.org/10.1017/jfm.2011.352 Published online by Cambridge University Press

straightforward description of shock waves. With respect to this, an important number of analytical results have been achieved in the last few years (e.g. Antuono, Hogg & Brocchini 2009; Antuono & Hogg 2009; Antuono 2010; Hogg, Baldock & Pritchard 2010) which complete and extend the pioneering work of Shen & Meyer (1963). Among these, the work by Antuono (2010) is the first which describes analytically the evolution of a shock wave from the seaward limit of the sloping beach up to the shoreline and, then, deals with the post-breaking evolution and the shock-induced run-up. These results have been obtained by assuming that one of the Riemann invariants of the NSWEs (specifically, that associated with signals entering the fluid region) is identically constant during the whole fluid motion. The Riemann invariants are functions which maintain constant along special curves, called characteristics. The assumption that one of the Riemann invariants is identically constant during the flow evolution enables the shock evolution to be modelled through an algebraic ordinary differential equation (ODE) system which is easy and fast to solve. The quasi-analytical solution obtained through numerical integration of this system is characterized by a single swash event followed by a sudden water withdrawal. Such a wave is uniquely associated with signals entering the fluid region.

Even if the results shown in Antuono (2010) have been applied to a shock wave propagating in still water, the solution is completely general and can be used to model a shock wave fed by a constant Riemann invariant which propagate into generic flow conditions. This aspect is of fundamental importance and is the main idea which lies under the present work. Indeed, it is possible to consider a series of shock waves each of these fed by a different constant Riemann invariant (§§ 3 and 4). In this way the solution by Antuono (2010) is still valid and a train of shock waves is generated.

The assignment of a piecewise-constant Riemann invariant at the seaward boundary corresponds to the assignment of purely incoming waves, that is, waves uniquely associated with signals entering the sloping region. These are characterized by a piecewise linear shape of the wave velocity and celerity at the seaward boundary. Consequently, the shock train displays a sawtooth profile that remains almost unchanged during the propagation towards the shore. This is an important feature since the same profile is observed for spilling breaking waves when they, shoreward of the breaking point (i.e. in the inner surf zone), reach a steady state (see, among many others, Svendsen 1994; Elgar & Guza 1985; Ting & Kirby 1994; Kaihatu *et al.* 2007; Abreu *et al.* 2010), and this information is often also used to model the near-bed sediment transport in the nearshore (e.g. Drake & Calantoni 2001; Suntoyo, Tanaka & Sana 2008).

A shock train solution may also have applications as a benchmark for numerical models of the nearshore flows, since it represents the first long-time quasi-analytical breaking solution for the NSWEs. The study of a shock train can be addressed to the validation of the numerical solvers based on the NSWEs (and on wave-resolving schemes in general). In one dimension these solvers are reliable and easy to use but they are generally tested against non-breaking solutions or breaking solutions that are valid for short-time intervals. In this context, the use of a long-time breaking solution may be of great importance. Then, the shock train solution may also provide useful results for wave-averaged models. In general, such models include physical phenomena which are not accounted for in the NSWE framework (e.g. dispersion due to flow non-uniformity in the vertical direction, turbulence). However, when these phenomena are neglected (by just switching off their contributions within the numerical solver), the mean (i.e. wave-averaged) quantities related to the shock train solution should

https://doi.org/10.1017/jfm.2011.352 Published online by Cambridge University Press

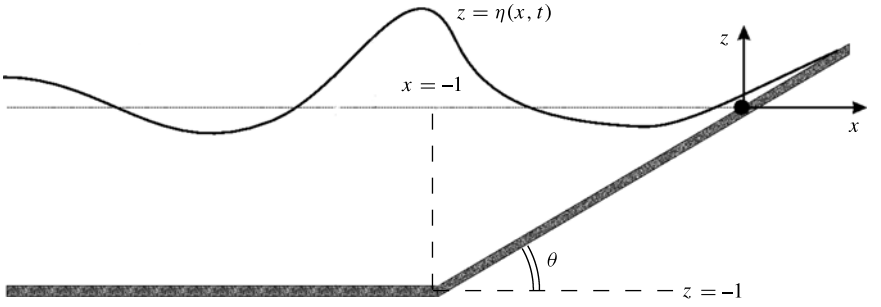


FIGURE 1. Sketch of geometry and flow dimensionless variables for the beach problem.

be recovered by the wave-averaged models. To this purpose, the final part of the present work is devoted to the inspection of the asymptotic behaviour of the shock train providing approximate analytical solutions and an overall description of the time-averaged quantities (§ 5). Moreover, an analysis of the energy dissipation caused by the asymptotic shock waves is provided.

2. The shock relations

For wave fronts approaching a uniformly sloping, frictionless beach with a small incident angle (Ryrie 1983; Brocchini & Peregrine 1996), the onshore problem of weakly two-dimensional NSWEs (in dimensionless form) is

$$\begin{cases} d_t + Q_x = 0, \\ Q_t + \left(\dfrac{d^2}{2} + \dfrac{Q^2}{d} \right)_x = h_x d, \end{cases} \tag{2.1}$$

in which $Q = ud$ is the onshore flux, u is the onshore velocity, $d = h + \eta$ is the total water depth, η is the free surface elevation, $h = -x$ is the still-water depth and subscripts give partial differentiation. The axes origin is posed at the undisturbed shoreline; the x coordinate gives the onshore direction and points in the landward direction (x, z) forming a right-handed Cartesian reference frame (see figure 1). The scale factors for vertical lengths, horizontal lengths and times are, respectively, the still-water depth at the seaward boundary $h_0^* = h^*(x = -1)$, $h_0^*/\tan\theta$ and $t_0^* = \sqrt{h_0^*/g}/\tan\theta$ where $\tan\theta$ is the beach slope, θ the angle of the plane beach with respect to the horizontal plane and the starred variables indicate dimensional variables. More details can be found in Brocchini & Peregrine (1996).

System (2.1) is hyperbolic and can be cast into its characteristic form by using the following variables

$$\alpha = u + t + 2c, \quad \beta = u + t - 2c, \tag{2.2}$$

where $c = \sqrt{d}$. Using α and β, the system (2.1) becomes

$$\begin{cases} \mathrm{d}\alpha/\mathrm{d}t = 0, & \text{on curves such that } \mathrm{d}x/\mathrm{d}t = u + c, \\ \mathrm{d}\beta/\mathrm{d}t = 0, & \text{on curves such that } \mathrm{d}x/\mathrm{d}t = u - c. \end{cases} \tag{2.3}$$

The curves defined in (2.3) are called characteristic curves (see, for example, Lax 1957; Toro 2001) and coincide at the shoreline where $c = 0$. When the flow is subcritical (that is, $u - c < 0 < u + c$), we call the former ones 'incoming', since

https://doi.org/10.1017/jfm.2011.352 Published online by Cambridge University Press

they move from the seaward boundary ($x=-1$) to the shoreline, and the latter ones 'outgoing', since they move toward the opposite direction. As pointed out by Antuono & Brocchini (2007), the former curves carry information on the incoming waves entering the seaward boundary while the latter curves carry information on the wave reflection at the shoreline. Note that α is constant along the incoming characteristic curves and β is constant along the outgoing curves. These functions are the so-called Riemann invariants (see, for example, Lax 1957; Jeffrey 1976; Leveque 2002) and are associated with incoming and reflected signals, respectively. Similarly to the characteristic curves, α and β coincide at the shoreline ($c=0$).

In the present work we consider a boundary value problem (BVP) including shock waves, that is, we solve the NSWEs assigning discontinuous wave signals at the seaward boundary of the domain (i.e. at $x=-1$). As discussed by Antuono & Brocchini (2007), the solution of the BVP for the NSWEs, is obtained by assigning the incoming Riemann invariant α at $x=-1$. This procedure intrinsically accounts for the reflection at the shoreline since the outgoing Riemann invariant β directly derives from the α datum. Indeed, the α datum is carried by the α characteristic curves towards the shoreline where $\beta=\alpha$ and the α characteristic curves coincide with the β characteristic curves. Then, these curves move back to the seaward boundary carrying the β values, that is, the reflected signals.

In the framework of hyperbolic systems, shock waves have to satisfy typical conservation properties (e.g. mass and momentum conservation). This leads to the so-called Rankine–Hugoniot relations (hereinafter simply called shock relations):

$$\begin{cases} s[\![d]\!] = [\![Q]\!], \\ s[\![Q]\!] = \left[\!\!\left[\dfrac{d^2}{2} + \dfrac{Q^2}{d} \right]\!\!\right], \end{cases} \tag{2.4}$$

where s is the shock wave velocity and $[\![f]\!]=f_2-f_1$ represents the jump of the quantity f across the discontinuity. The subscript '2' indicates the values seaward of the shock wave while '1' indicates the values shoreward of the shock wave.

As widely known in the literature (see, for example, Lax 1957; Whitham 1974; Leveque 2002), shock relations are not sufficient to find the solution univocally. As a consequence, further conditions (called entropy conditions in analogy with the gas-dynamics theory) are introduced to recover the uniqueness of the solution. For a shock wave generated by the collapse of the incoming characteristic curves, the entropy conditions prescribe

$$u_1 + c_1 \leqslant s \leqslant u_2 + c_2, \tag{2.5}$$

and these enable rewriting the shock relations as

$$s = u_1 + \sqrt{\frac{1}{2}\left(\frac{d_2^2}{d_1} + d_2\right)} \quad \text{or} \quad s = u_2 + \sqrt{\frac{1}{2}\left(\frac{d_1^2}{d_2} + d_1\right)}, \tag{2.6}$$

and

$$d_2 = -\frac{d_1}{2} + \frac{1}{2}\sqrt{d_1^2 + 8d_1(s-u_1)^2}. \tag{2.7}$$

Further, it is $d_1 \leqslant d_2$ and $u_1 \leqslant u_2$.

https://doi.org/10.1017/jfm.2011.352 Published online by Cambridge University Press

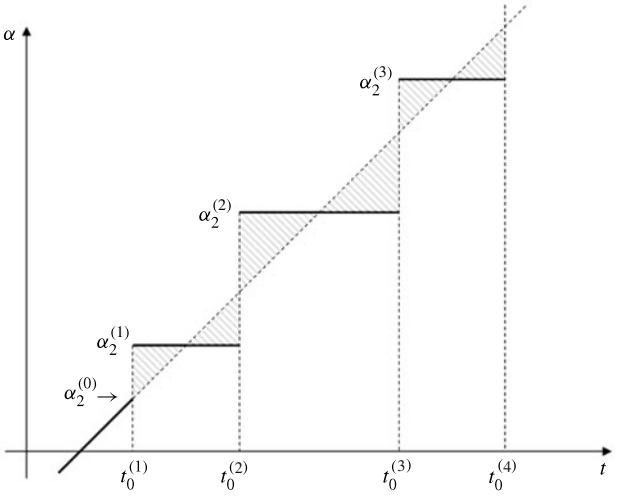


FIGURE 2. Sketch of the datum α at $x = -1$ (thick solid lines). The shaded volumes measure the discrepancy with respect to the still water solution $\alpha = 2 + t$.

3. The α-constant shock train

In Antuono (2010) a quasi-analytical solution for the propagation of a shock wave is derived. This is based on the assumption that the flow field seaward the shock is characterized by a constant incoming Riemann invariant α. To enforce such a condition it is sufficient to impose $\alpha =$ constant at the seaward boundary of the domain (that is, at $x = -1$). Owing to the first equation in (2.3), each incoming characteristic curve carries a specific value of α from the seaward boundary inside the sloping region without altering it. Consequently, the constancy of α at the seaward boundary results into the constancy of α inside the whole fluid domain.

This solution can be generalized in a straightforward way to get a sequence of shock waves followed by an α-constant field. In this case the datum α at the seaward boundary of the domain has to be piecewise continuous (see figure 2) and each discontinuity corresponds to a shock wave entering the sloping region. In the following such a sequence is called an α-constant shock train.

Now, let us assume that the solution along the $(n-1)$th shock of the train is known and focus on the nth shock. The α field along the seaward side is known through the seaward boundary assignment. Conversely, all of the quantities on the shoreward side are obtained through the solution of the previous shock wave. In fact, after the solution along the seaward side of the $(n-1)$th shock wave is known, the β characteristic curves (second equation in (2.3)) are used to propagate the values of β up to the shoreward side of the nth shock (see figure 3). Here, the value of α is known through the seaward boundary assignment and, using (2.2), it is possible to compute the water depth and velocity. This procedure is schematically displayed in figure 3. After this, the solution of the nth α-constant shock wave is obtained through the following algebraic ODE system:

$$\frac{\mathrm{d}x^{(n)}}{\mathrm{d}t} = s^{(n)} = u_1^{(n)} + \sqrt{\frac{1}{2}\left[\frac{(d_2^{(n)})^2}{d_1^{(n)}} + d_2^{(n)}\right]} \tag{3.1}$$

https://doi.org/10.1017/jfm.2011.352 Published online by Cambridge University Press

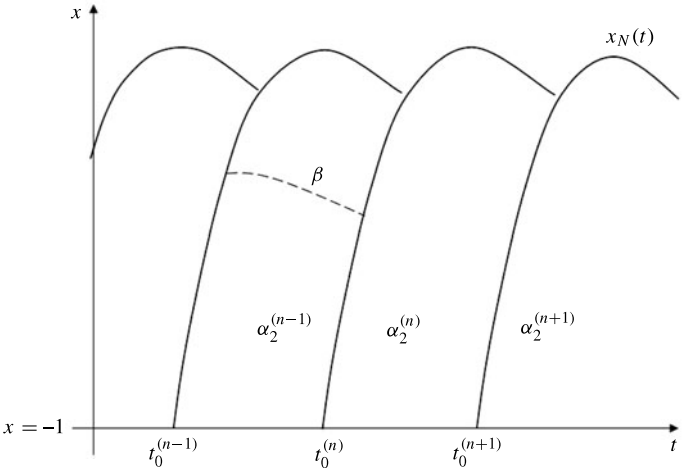


FIGURE 3. Sketch of the α-constant shock train. The dashed line represents a β characteristic curve which emanates from the $(n-1)$th shock wave and reaches the nth shock wave. The symbol $x_N(t)$ represents the shoreline.

and the correct solution for $d_2^{(n)}$ is obtained through the following sixth-order polynomial:

$$z^6 - 9c_1^{(n)}z^4 + 8\sqrt{c_1^{(n)}}[\alpha_2^{(n)} - \alpha_1^{(n)} + 2c_1^{(n)}]z^3 - [2(\alpha_2^{(n)} - \alpha_1^{(n)} + 2c_1^{(n)})^2 + (c_1^{(n)})^2]z^2 + (c_1^{(n)})^3 = 0, \tag{3.2}$$

where $z = c_2^{(n)}/\sqrt{c_1^{(n)}}$ and $c_i^{(n)} = \sqrt{d_i^{(n)}}$ for $i = 1, 2$. The superscript (n) indicates all of the quantities associated with the nth shock wave. The polynomial above is obtained by combining (2.6) with (2.7) and the correct root is that satisfying the entropy conditions in (2.5). Note that, in agreement with the hypotheses made above, it is $\alpha_1^{(n)} = \alpha_2^{(n-1)}$ (see figure 3).

The choice of the datum α at the seaward boundary needs some care. Indeed, notwithstanding the condition $\alpha =$ constant can be achieved in different ways, some of those can lead to solutions characterized by strong variations of the volume of water in the sloping region. In the present work we do not deal with them but focus on 'regular' trains on shores, that is, shock trains which induce small variations of the volume of water. To do this, we require that the boundary datum has a null integral mean with respect to the still water solution at the seaward boundary, that is $\alpha = 2 + t$. In some sense, this is equivalent to require that the 'volume' of information coming from the seaward boundary is not characterized by any mean excess/lack with respect to the still water case. This condition is very general and allows for a wide range of boundary data. In the specific, in the present work we apply such a condition to each single shock event entering the sloping region (see, for example, figure 2). This leads to the following relation between the jump of α and the interval between two subsequent shock waves:

$$\Delta t^{(2)} = 2\Delta\alpha^{(1)}, \quad \Delta t^{(n+1)} = 2\Delta\alpha^{(n)} - \Delta t^{(n)}, \tag{3.3}$$

where $\Delta t^{(n)} = t_0^{(n)} - t_0^{(n-1)}$ ($t_0^{(n)}$ being the instant at which the nth shock enters the sloping region) and $\Delta\alpha^{(n)} = \alpha_2^{(n)} - \alpha_1^{(n)} = \alpha_2^{(n)} - \alpha_2^{(n-1)}$. Figure 4 shows two

https://doi.org/10.1017/jfm.2011.352 Published online by Cambridge University Press

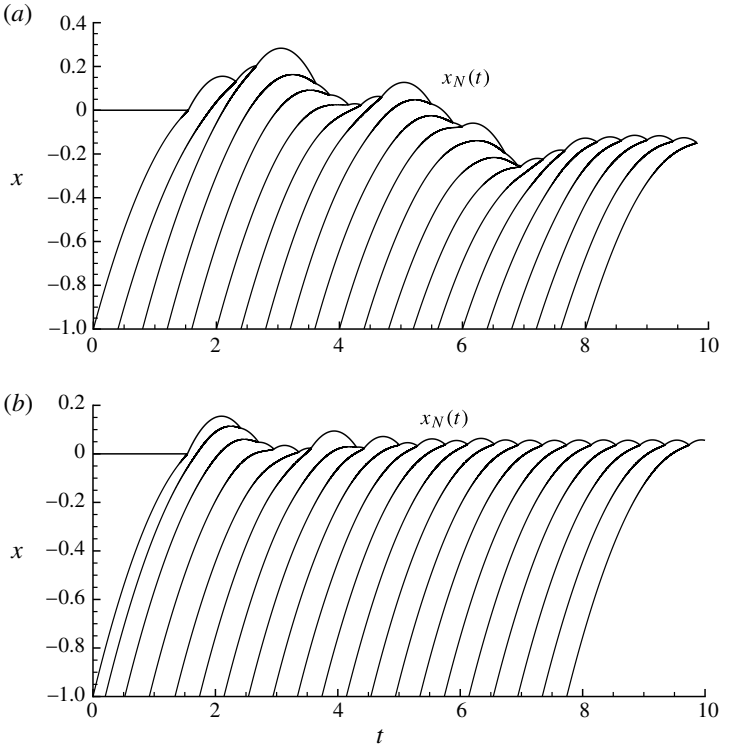


FIGURE 4. Case (*a*), shock train which does not satisfy relation (3.3). Case (*b*), shock train satisfying relation (3.3).

different α-constant shock trains, cases (*a*) and (*b*), which start from still water conditions. Case (*a*) (top panel) does not satisfy relation (3.3) and, therefore, is characterized by strong variations of the volume of water in the sloping region. In the specific, a decrease of the water level is observed. Conversely, case (*b*) (lower panel) satisfies the relation in (3.3) and shows a very regular shock pattern. In any case, a deeper analysis of the relation between the boundary data and the variation of the water volume is provided in § 5.1. The initial data of the shock trains in figure 4 are provided in tables 1 and 2. Since both cases start from still water conditions, it is $\alpha_2^{(0)} = 2 + t_0^{(1)}$, with $\alpha_2^{(0)}$ being the value of α on the shoreward side of the first shock event. The specific choices of Δt and $\Delta\alpha$ are made to avoid shock merging and/or the shock withdrawal up to the seaward boundary. The former case occurs when a shock wave is too strong in comparison with the previous one. Conversely, the latter case occurs when a shock wave is so weak that it is led out of the sloping region by the flow field induced by the previous shock wave.

In figure 5 the water depth and the water velocity at fixed x positions are displayed for the shock train of case (*b*). In the specific, the first 10 shock waves are considered since the global behaviour for longer times does not significantly deviate from the last shock events of figure 5. As expected, the wave signals at $x = 0$ show larger displacements from the still water solution during the initial shock events while a more regular behaviour appears for longer times. The maximum velocity is obtained when the first shock wave reaches the still shoreline and is associated with the maximum run-up of the wave train (see the lower panel of figure 4). Conversely, the wave signals

https://doi.org/10.1017/jfm.2011.352 Published online by Cambridge University Press

n	$t_0^{(n)}$	$\alpha^{(n)}$	n	$t_0^{(n)}$	$\alpha^{(n)}$
1	0.0	2.10	11	4.00	6.17
2	0.4	2.70	12	4.40	6.52
3	0.8	3.05	13	4.80	6.86
4	1.2	2.10	14	5.20	7.22
5	1.6	2.10	15	5.60	7.60
6	2.0	2.10	16	6.00	8.00
7	2.4	2.10	17	6.40	8.40
8	2.8	2.10	18	6.80	8.80
9	3.2	2.10	19	7.20	9.20
10	3.6	2.10	20	7.60	9.60

TABLE 1. Initial data for the shock trains described in the upper panel of figure 4.

n	$t_0^{(n)}$	$\alpha^{(n)}$	n	$t_0^{(n)}$	$\alpha^{(n)}$
1	0.00	2.10	11	3.74	5.94
2	0.20	2.36	12	4.14	6.34
3	0.52	2.72	13	4.54	6.74
4	0.92	3.13	14	4.94	7.14
5	1.34	3.54	15	5.34	7.54
6	1.74	3.94	16	5.74	7.94
7	2.14	4.34	17	6.14	8.34
8	2.54	4.74	18	6.54	8.74
9	2.94	5.14	19	6.94	9.14
10	3.34	5.54	20	7.34	9.54

TABLE 2. Initial data for the shock trains described in the lower panel of figure 4.

at the seaward boundary ($x = -1$) and inside the sloping region ($x = -0.5$) show a rapid convergence to a sawtooth profile. This shape is similar to that observed for spilling breaking waves when they reach a steady state, that is, when they resemble a bore (see, for example, Svendsen 1994). Further, the sawtooth profile is in good agreement with that predicted using the definition of 'incoming' and 'reflected' components of the boundary data introduced by Antuono & Brocchini (2007) and, then, further inspected in Antuono (2010). This concept is based on the following decomposition at the seaward boundary (that is, at $x = -1$):

$$c(-1,t) = 1 + c^I(t) + c^R(t) \quad u(-1,t) = u^I(t) + u^R(t), \tag{3.4}$$

where the superscript 'I' indicates the incoming components and 'R' indicates the reflected components. The incoming components are univocally associated with the variable α and satisfy $u^I = 2c^I$. Conversely, the reflected components are univocally associated with the variable β and satisfy $u^R = -2c^R$. Extending the results found by Antuono (2010) under the assumption that α is constant, it follows that

$$c^I(t) = \frac{\alpha(-1,t) - 2 - t}{4} \quad \forall t > 0. \tag{3.5}$$

Since $\alpha(-1,t)$ is piecewise continuous (see figure 2), both c^I and u^I show a sawtooth profile. Figure 6 shows the reflected components c^R and u^R for the case (b) shock

https://doi.org/10.1017/jfm.2011.352 Published online by Cambridge University Press

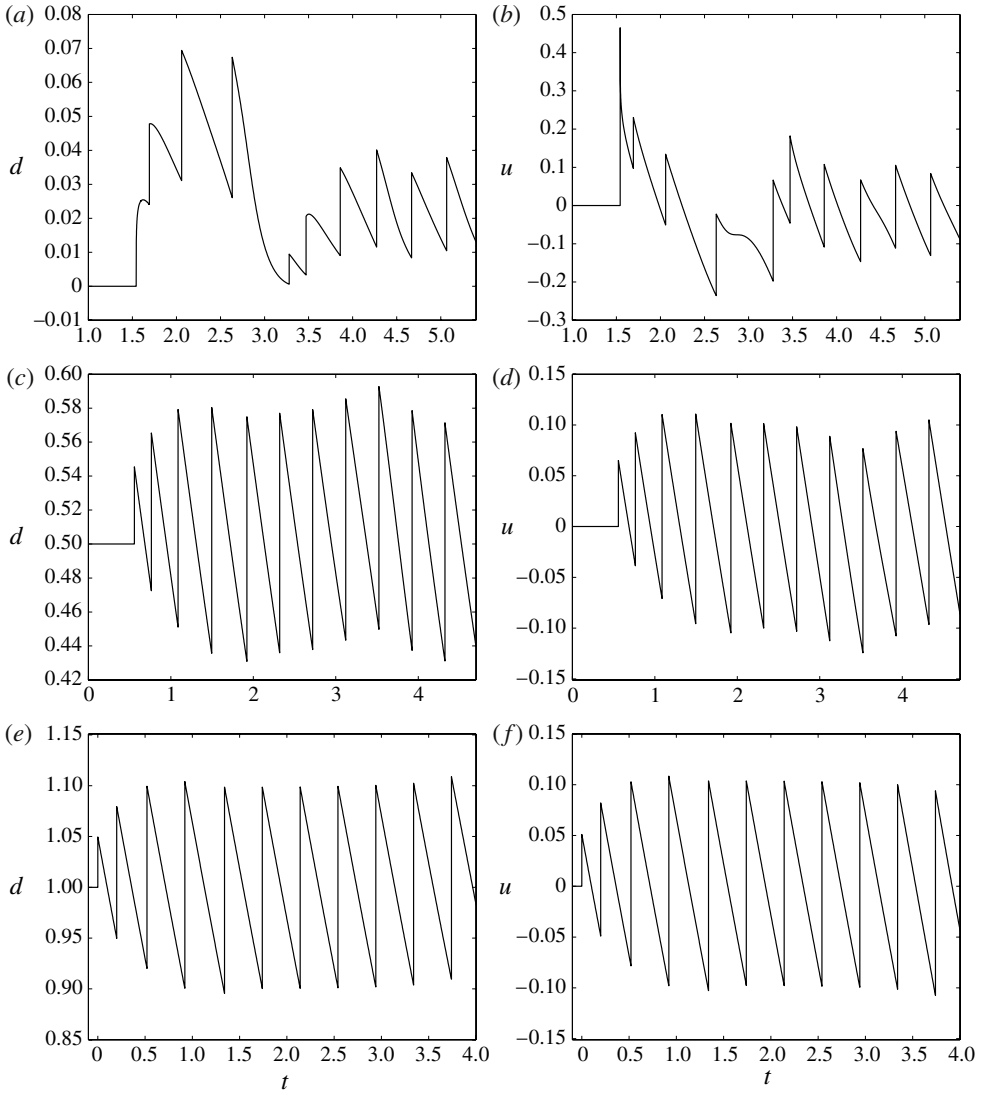


FIGURE 5. Water depth and water velocity of the case (*b*) shock train at fixed *x*-coordinates: (*a*,*b*) $x = 0$; (*c*,*d*) $x = -0.50$; (*e*,*f*) $x = -1.0$.

train. These have been computed using the numerical outputs illustrated in the lower panels of figure 5 and subtracting the incoming components in (3.5) according to the definition given in (3.4). As predicted in Antuono (2010), they satisfy the relation $u^R = -2c^R$. Since c^R and u^R are of order $O(10^{-3})$, the numerical outputs at the seaward boundary are almost coincident with the incoming components. This means that c^I and u^I can both be used in numerical solvers for the assignment at the seaward boundary, that is, we can assume $c \simeq 1 + c^I$ and $u \simeq u^I$.

4. Numerical details

In this section we briefly describe the algorithm used to obtain the shock train solutions. First, we assume the $(n-1)$th shock to be known, that is, we assume that

https://doi.org/10.1017/jfm.2011.352 Published online by Cambridge University Press

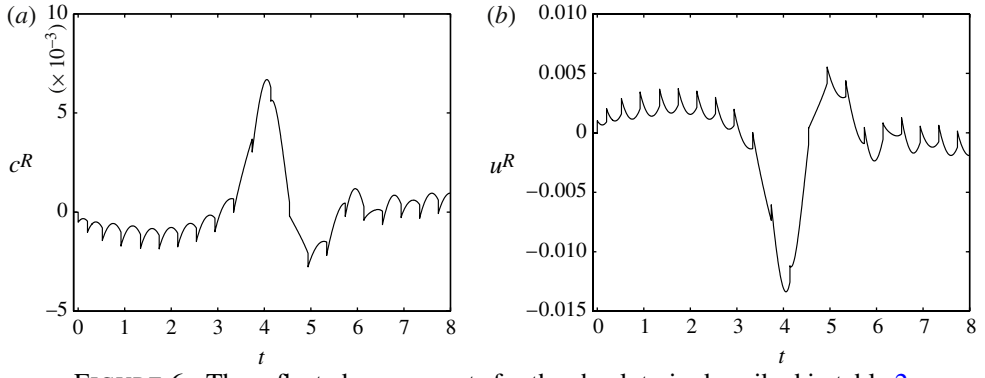


FIGURE 6. The reflected components for the shock train described in table 2.

all quantities along its seaward side are known. Then, to solve the nth shock wave through the algebraic ODE system in (3.1) and (3.2), we first need to compute all of the flow quantities between the $(n-1)$th and the nth shock wave (we recall that the data $\alpha_2^{(n-1)}$ and $\alpha_2^{(n)}$ are known by assignment). In the specific, it is sufficient to find out the value of β at a generic point (x,t) between the $(n-1)$th and the nth shock waves. Then, using $\beta(x,t)$ and $\alpha_2^{(n-1)}$, we get the flow field ahead of the nth shock through the following relations:

$$u(x,t)=\frac{\alpha_2^{(n-1)}+\beta(x,t)}{2}-t,\quad c(x,t)=\frac{\alpha_2^{(n-1)}-\beta(x,t)}{4}. \tag{4.1}$$

To find $\beta(x,t)$ we proceed as follows. First, using (2.2), we rewrite the second expression of (2.3) in the following way:

$$\frac{\mathrm{d}x}{\mathrm{d}t}=\left(\frac{\alpha_2^{(n-1)}+3\beta}{4}-t\right)\quad \text{on curves such that } \beta=\text{constant}, \tag{4.2}$$

and, integrating, we obtain

$$x=x_s^{(n-1)}+\left(\frac{\alpha_2^{(n-1)}+3\beta}{4}\right)(t-t_s^{(n-1)})-\frac{t^2}{2}+\frac{(t_s^{(n-1)})^2}{2}, \tag{4.3}$$

where $(t_s^{(n-1)},x_s^{(n-1)})$ denotes the point along the $(n-1)$th shock wave intersected by the specific β characteristic curve. A straightforward representation of the shock wave provides $t_s^{(n-1)}$ as an independent variable and x_s,β as dependent variables. However, as proved in Antuono (2010), it is possible and more convenient to use β as an independent variable and write $t_s^{(n-1)}=t_s^{(n-1)}(\beta)$ and, consequently, $x_s^{(n-1)}=x_s^{(n-1)}(\beta)$. This means that both $t_s^{(n-1)}$ and $x_s^{(n-1)}$ univocally depend on the chosen value of β. As a consequence of this choice, (4.3) only depends on x,t and β. As proved in Antuono (2010) for each pair (t,x) with $t\geqslant t_s^{(n-1)}(\beta)$, it is possible to make β explicit (that is, $\beta=\beta(t,x)$) and this solution is unique. This implies that, for a fixed pair (x,t), the specific value of $\beta(t,x)$ is simply obtained by evaluating numerically the (unique) zero of

$$\phi(\beta)=-x+x_s^{(n-1)}(\beta)+\left(\frac{\alpha_2^{(n-1)}+3\beta}{4}\right)(t-t_s^{(n-1)}(\beta))-\frac{t^2}{2}+\frac{(t_s^{(n-1)}(\beta))^2}{2} \tag{4.4}$$

for $t\geqslant t_s^{(n-1)}(\beta)$.

https://doi.org/10.1017/jfm.2011.352 Published online by Cambridge University Press

After the flow quantities along the shoreward side of the nth shock are computed, polynomial (3.2) is used to obtain $d_2^{(n)}$. The correct root is obtained by using a simple bisection method and noting that it must lie in the following range:

$$\sqrt{c_1^{(n)}} \leqslant z \leqslant \frac{2(\Delta\alpha^{(n)} + c_1^{(n)})}{\sqrt{c_1^{(n)} + \sqrt{9(c_1^{(n)})^2 + 8(\Delta\alpha^{(n)})^2 + 16c_1^{(n)}\Delta\alpha^{(n)}}}}. \tag{4.5}$$

A detailed proof of the bounds above is given in Appendix A.

Finally, the value of $d_2^{(n)}$ is used to solve the ODE (3.1). In the specific, a fourth-order Runge–Kutta scheme has been used. The time step to be used as a reference inside the four sub-steps of the Runge–Kutta scheme is given by

$$\mathrm{d}t^{(1)} = \tau_0[1 - (1 - d_1^{(1)})^\gamma], \quad \text{with } \gamma = 12, \tau_0 = 10^{-4}, \tag{4.6}$$

for the first shock event (that is, the shock propagating in still water) while

$$\mathrm{d}t^{(n)} = \tau_0\sqrt{d_1^{(n)}}, \quad \text{with } \tau_0 = 10^{-4}, \tag{4.7}$$

for the subsequent shock waves. The specific value of τ_0 guarantees a fine discretization of the shock wave (∼30 000 points for each shock event). The dependence of $\mathrm{d}t^{(n)}$ on $d_1^{(n)}$ is motivated by the request for a higher accuracy as the shock wave moves shoreward (that is, as d_1 goes to zero). The specific structure of such a dependence is needed to make the solution go up to $d_1^{(n)} = O(10^{-12})$ near the shoreline (for lower values of $d_1^{(n)}$ the computation is stopped). The request for $d_1^{(n)} = O(10^{-12})$ near the shoreline is due to the fact that the accuracy on the seaward side of the shock wave is, generally, smaller. In fact, as a consequence of the results found in Antuono (2010), it is $d_2^{(n)} \simeq \sqrt{d_1^{(n)}} = O(10^{-6})$ and $c_2^{(n)} = \sqrt{d_2^{(n)}} = O(10^{-3})$ near the shoreline.

This behaviour is also the cause of a numerical issue which affects the solution for the shock trains. Indeed, if we choose $d_1^{(1)} = O(10^{-12})$ as a threshold depth for the first shock wave, we would get $d_2^{(1)} = O(10^{-6})$ on the seaward side. When the flow field in front of the second shock wave is computed, this would imply $d_1^{(2)} = O(10^{-6})$ and, therefore, $d_2^{(2)} = O(10^{-3})$ on the seaward side. As a consequence, we would have lower and lower accuracy at the shoreline as new shock waves are solved. To avoid this problem, for each shock event we use the generalized Shen & Meyer (1963) solution described in Antuono (2010) to 'extend' the depth on the shoreward side from $d_1^{(n)} = O(10^{-6})$ to $d_1^{(n)} = O(10^{-12})$. The generalized Shen & Meyer (1963) solution is an asymptotic solution valid in the neighbourhood of the shoreline. It is given by

$$d(x, t) = \frac{(x - x_N(t))^2}{9(t - t_{s,N}^{(n)})^2}, \tag{4.8}$$

where

$$x_N(t) = x_{s,N}^{(n)} + \alpha_2^{(n)}(t - t_{s,N}^{(n)}) - \frac{t^2}{2} + \frac{1}{2}(t_{s,N}^{(n)})^2, \tag{4.9}$$

is the shoreline and $x_{s,N}^{(n)}$ and $t_{s,N}^{(n)}$ are the x and t coordinates at which the nth shock reaches the shoreline. The corresponding solution for the water velocity is obtained

https://doi.org/10.1017/jfm.2011.352 Published online by Cambridge University Press

through

$$u(x,t) = \alpha_2^{(n)} - 2\sqrt{d(x,t)} - t. \tag{4.10}$$

Note that the use of the generalized Shen & Meyer (1963) solution is motivated only by numerical reasons and does not alter the validity of the shock train solution.

5. Asymptotically periodic shock trains

In this section we study shock trains which satisfy condition (3.3) and which asymptotically converge towards a periodic solution. This means that, for a long enough time, each shock event has to be identical to the previous one except for an unessential time translation. To attain such a behaviour, we first need to achieve an asymptotically periodic assignment at the seaward boundary. Denoting by

$$\Delta\alpha = \lim_{n\to+\infty} \Delta\alpha^{(n)} \quad \text{and} \quad \Delta t = \lim_{n\to+\infty} \Delta t^{(n)}, \tag{5.1}$$

condition (3.3) gives $\Delta t = \Delta\alpha$ and Δt is the asymptotic period of the shock train. For example, the case (b) shock train has $\Delta\alpha = 0.4$ and the asymptotic assignment at the seaward boundary is reached after the sixth shock event. Notwithstanding that, the asymptotic solution takes a much longer time to be attained since each shock event is influenced and disturbed by the previous events.

In figure 7 the free-surface elevation and the water velocity of this shock train are displayed at $t = 30.59$ and $t = 30.79$ (that is, just after the 78th shock event enters the sloping region). The solution can be regarded as approximatively periodic since the time variation of the mean quantities is very small (more details are given in the next section). The free surface as well as the velocity display a sawtooth profile all over the sloping region with a relatively small distortion near the shoreline. The jump in the water depth decreases almost linearly as shock waves move shoreward while the jump in the velocity keeps almost constant with a slight increase just seaward of the shoreline.

In § 5.1 we deal with the asymptotic conditions to be satisfied by the periodic shock train and with the energy dissipation induced by the shock events. However, before proceeding to the analysis, we define the following variable:

$$A^{(n)} = \frac{\alpha^{(n)} + \alpha^{(n-1)}}{2}, \tag{5.2}$$

which represents the mean of the α values along the seaward and shoreward side of the nth shock. In Appendix B we prove that, for large values of n and for shock trains starting from still water conditions (such as those described here), the following asymptotic relation holds true:

$$t_0^{(n)} = A^{(n)} - 2 \quad \text{for } n \text{ large}. \tag{5.3}$$

Under the same hypothesis, formulae (5.1) and (5.3) permit us to obtain the asymptotic expressions of c^I and u^I:

$$c^I = \frac{\Delta\alpha - 2\tau}{8} \quad u^I = \frac{\Delta\alpha - 2\tau}{4}, \tag{5.4}$$

where $\tau = t - t_0^{(n)}$ (note that $\tau \in [0, \Delta\alpha]$).

https://doi.org/10.1017/jfm.2011.352 Published online by Cambridge University Press

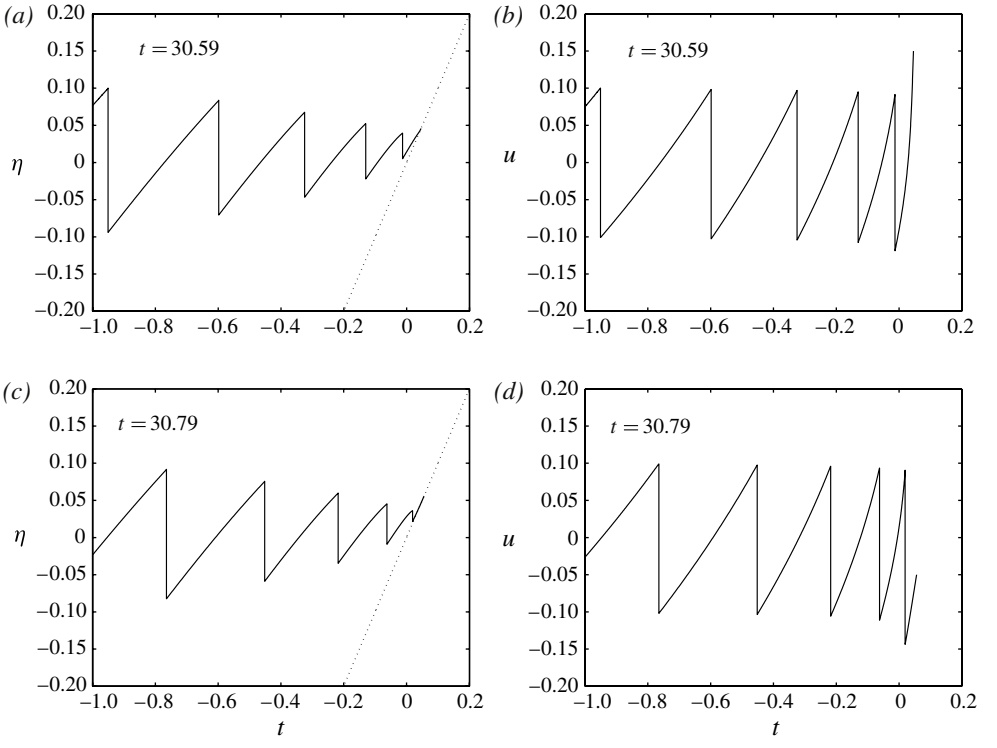


FIGURE 7. Long-time evolution for the case (*b*) shock train ($\Delta\alpha = 0.4$): (*a*,*c*) the free-surface elevation (solid lines) and the beach bottom (dotted lines); (*b*,*d*) the water velocity.

5.1. *Integral equations and shock-induced dissipation*

In the following we provide a simple analysis of periodic solutions based on a space/time average of the NSWEs. Before proceeding, we add to system (2.1) the equation of the total energy in its conservative form (see the Appendix C):

$$\left(\frac{Q^2}{2d} + \frac{\eta^2}{2}\right)_t + \left(\frac{Q^3}{2d^2} + \eta Q\right)_x = 0. \tag{5.5}$$

Let us integrate the NSWEs and the energy equation for $-1 \leqslant x \leqslant x_N(t)$ and, then, for t in $[t, t+T]$. Imposing the solution to be periodic with period T, we obtain

$$\begin{cases} \langle Q_0 \rangle = 0 \\ \langle V \rangle = \left\langle \left[\dfrac{Q_0^2}{d_0} + \dfrac{d_0^2}{2} \right] \right\rangle \\ \langle \mathscr{D} \rangle = \left\langle \left[\dfrac{Q_0^3}{2d_0^2} + \eta_0 Q_0 \right] \right\rangle \end{cases} \tag{5.6}$$

where the brackets $\langle . \rangle$ indicate the mean over a period, the subscript 0 denotes the quantities at the seaward boundary ($x = -1$), V is the water volume in the sloping region and, finally, $\mathscr{D}$ is the dissipation caused by the shock waves. Before proceeding to the analysis, we underline that system (5.6) is approximatively valid also when the time variations of the mean quantities are negligible, that is, when the solution

https://doi.org/10.1017/jfm.2011.352 Published online by Cambridge University Press

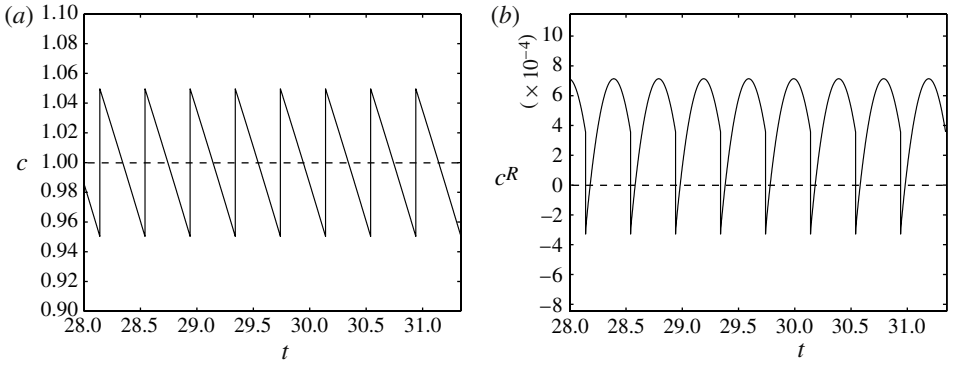


FIGURE 8. The wave celerity (a) and its reflected component (b) for the case (b) shock train (see figure 4b) after 75 shock events (the 75th shock event starts at $t = 29.34$). The dashed lines indicate the still water solution. All signals are computed at the seaward boundary $x = -1$.

is approximatively periodic. All details of derivations are provided in Appendix C. The first equation in (5.6) provides a necessary condition for the attainment of the asymptotic solution, that is, the mean volume flux across the seaward boundary must be zero. The second equation gives the asymptotic value of the water volume in the sloping region (note that the volume in still water conditions is equal to $1/2$). Finally, the third equation states that the energy dissipation caused by a single shock event must equal the mean energy flux across the seaward boundary.

Now, we give an estimate of the seaward boundary quantities in (5.6). We first assume that the reflected components are much smaller than the incoming components. This is suggested by figure 8 where the seaward boundary is displayed after 75 shock events. Denoting through ϵ and δ the orders of magnitude of the incoming and reflected components respectively, we have

$$u^I = 2c^I,\ c^I = O(\epsilon) \quad u^R = -2c^R,\ c^R = O(\delta) \quad \text{with } \delta \ll \epsilon \ll 1. \tag{5.7}$$

From the expression of the incoming velocity in (5.4) it follows that $\epsilon = \Delta\alpha/2$. The second assumption is that $\langle c^R \rangle \neq 0$. Again, this is suggested by figure 8 and, as shown in the following, it is needed to satisfy the condition $\langle Q_0 \rangle = 0$. These assumptions imply

$$\begin{cases} \langle Q_0 \rangle = \dfrac{(\Delta\alpha)^2}{48} - 2\langle c^R \rangle + O(\epsilon^2\delta, \delta^2), \\ \langle V \rangle = \dfrac{1}{2} + \dfrac{7(\Delta\alpha)^2}{192} + \dfrac{9(\Delta\alpha)^4}{40\,960} + 2\langle c^R \rangle + O(\epsilon\delta, \delta^2), \\ \langle \mathscr{D} \rangle = \dfrac{(\Delta\alpha)^2}{24} + \dfrac{3(\Delta\alpha)^4}{3840} - 2\langle c^R \rangle + O\left(\epsilon^4\delta, \delta^2\right). \end{cases} \tag{5.8}$$

Imposing $\langle Q_0 \rangle = 0$, we obtain $\langle c^R \rangle = (\Delta\alpha)^2/96$, that is, $\delta = \epsilon^2$ which is consistent with the initial assumption on the order of magnitude of the reflected components. Then, at the leading order we obtain

$$\langle V \rangle = \frac{1}{2} + \frac{11}{192}(\Delta\alpha)^2 + O(\epsilon^3), \quad \langle \mathscr{D} \rangle = \frac{(\Delta\alpha)^2}{48} + O(\epsilon^4). \tag{5.9}$$

Obviously, these formulae are increasingly accurate as ϵ becomes smaller and smaller.

https://doi.org/10.1017/jfm.2011.352 Published online by Cambridge University Press

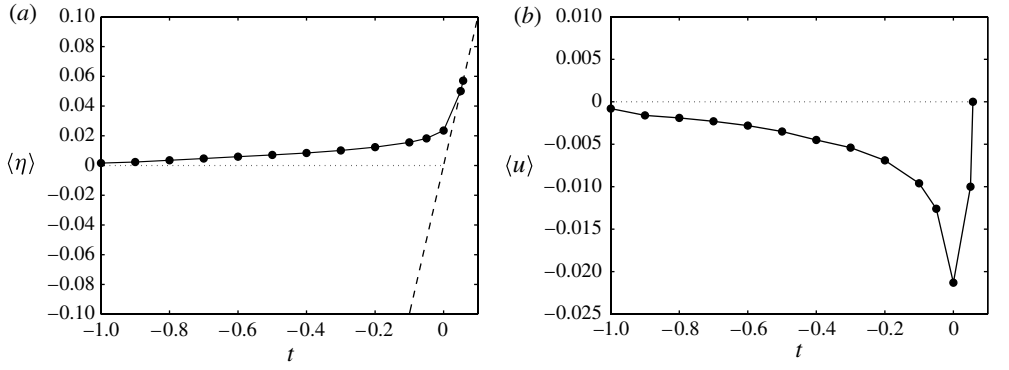


FIGURE 9. Mean surface elevation and mean velocity of the case (*b*) shock train after 25 shock events. Dotted lines indicate the still water conditions while the dashed line represents the beach bottom.

	After 25 shock events	After 75 shock events	Asymptotic values
$\langle Q_0 \rangle$	2.51×10^{-3}	2.42×10^{-3}	0
$\langle V \rangle - 1/2$	6.67×10^{-3}	6.76×10^{-3}	$\simeq 9.1 \times 10^{-3}$
$\langle \mathscr{D} \rangle$	5.86×10^{-3}	5.77×10^{-3}	$\simeq 3.3 \times 10^{-3}$
$\langle c^R \rangle$	4.10×10^{-4}	4.55×10^{-4}	$\simeq 1.6 \times 10^{-3}$

TABLE 3. Time-averaged quantities for the case (*b*) shock train ($\Delta\alpha = 0.4$).

In table 3 the time-averaged quantities of the case (*b*) shock train are computed after 25 and 75 shock events. The integration is made over 5 shock events (i.e. quantities related to the 25th shock wave have been computed by using shocks from 23 rd to 27th). This shock train is characterized by $\Delta\alpha = 0.4$ (that is, $\epsilon = 0.2$) and, therefore, represents a strongly nonlinear case (see, for example, figure 7). The computed values are in good agreement with the leading-order analytical relations of system (5.8) but are quite different from the asymptotic values shown in the fourth column of table 3. This implies that the asymptotic solution is not attained yet. However, the fact that system (5.8) is satisfied at the leading order means that the time variation of the mean quantities is extremely small and that the solution can be regarded as approximatively periodic. This is confirmed by the second and third columns of table 3 and by inspection of the numerical solution. In the specific, after the 15th shock event the solution can be practically regarded as periodic.

In figure 9 the mean surface elevation and mean velocity are displayed for the same train after 25 shock events (all quantities have been computed by using shocks from 23th to 27th). An increase of the mean water level $\langle \eta \rangle$ is observed all over the sloping region. As expected, this grows towards the shore where it is rather pronounced. Conversely, the mean velocity $\langle u \rangle$ is characterized by a more complex profile with a minimum at the still shoreline position ($x = 0$) and remains negative all over the fluid domain.

https://doi.org/10.1017/jfm.2011.352 Published online by Cambridge University Press

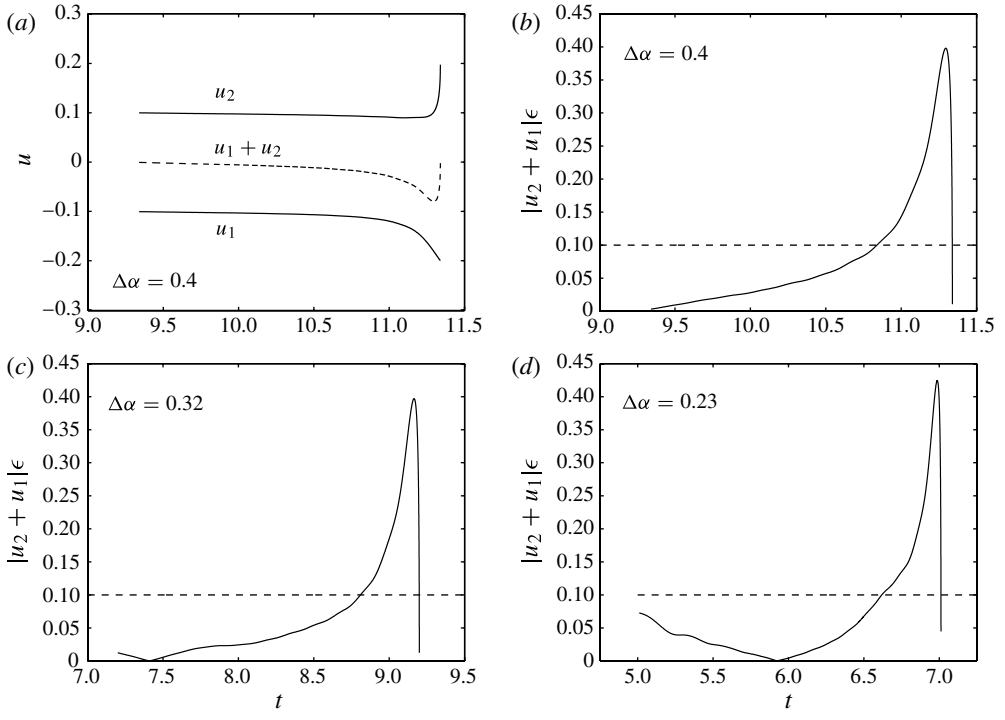


FIGURE 10. (*a*) Seaward and shoreward velocity along the 25th shock wave ($\Delta\alpha = 0.4$). (*b–d*) $|u_2 + u_1|/\epsilon$ along the 25th shock for different values of $\Delta\alpha$.

5.2. *Approximate asymptotic solution: a conjecture*

In the previous section, the asymptotic behaviour of the periodic shock train has been studied by analysing the mean quantities which characterized it. Here, we provide an approximate asymptotic solution for the shock wave which is based on a conjecture about the velocity field distribution along it.

Let us consider figure 10. In the top left panel the seaward and shoreward velocities are displayed along the 25th shock wave of case (*b*) ($\Delta\alpha = 0.4$). Their signs are opposite but their profiles are very similar. This behaviour is reached after ∼15–20 shock events and remains unchanged during the subsequent evolution (at least until the 75th shock event which is the last shock event inspected). Further, it appears almost identical for shock trains characterized by different values of $\Delta\alpha$. This seems to indicate that the sum $(u_2 + u_1)$ remains small asymptotically. To quantify this aspect, the remaining panels of figure 10 display the quantity $|u_2 + u_1|/\epsilon$ showing that it remains smaller than 0.1 during most of the shock evolution. A larger (but temporally limited deviation from 0.1) is observed in the neighbourhood of the shoreline position. However, it always remains smaller than 0.4.

Starting from these observations, we assume the following conjecture to hold asymptotically, that is, $|u_2 + u_1|/\epsilon \ll 1$. Thanks to this assumption, we are able to find an implicit asymptotic solution for the shock wave evolution. Denoting $u_2 = -u_1 = \upsilon$ and $\tau = t - t_0^{(n)}$, we obtain

$$2 - \tau = \frac{\Delta\alpha}{2}\frac{\kappa}{\kappa+1}\left(\frac{2+\kappa^2+\kappa\sqrt{\kappa^2+8}}{2(1-\kappa^2)}\right)^{1/2} \quad \text{with } \kappa = \frac{\Delta\alpha}{2\upsilon} - 1 \tag{5.10}$$

https://doi.org/10.1017/jfm.2011.352 Published online by Cambridge University Press

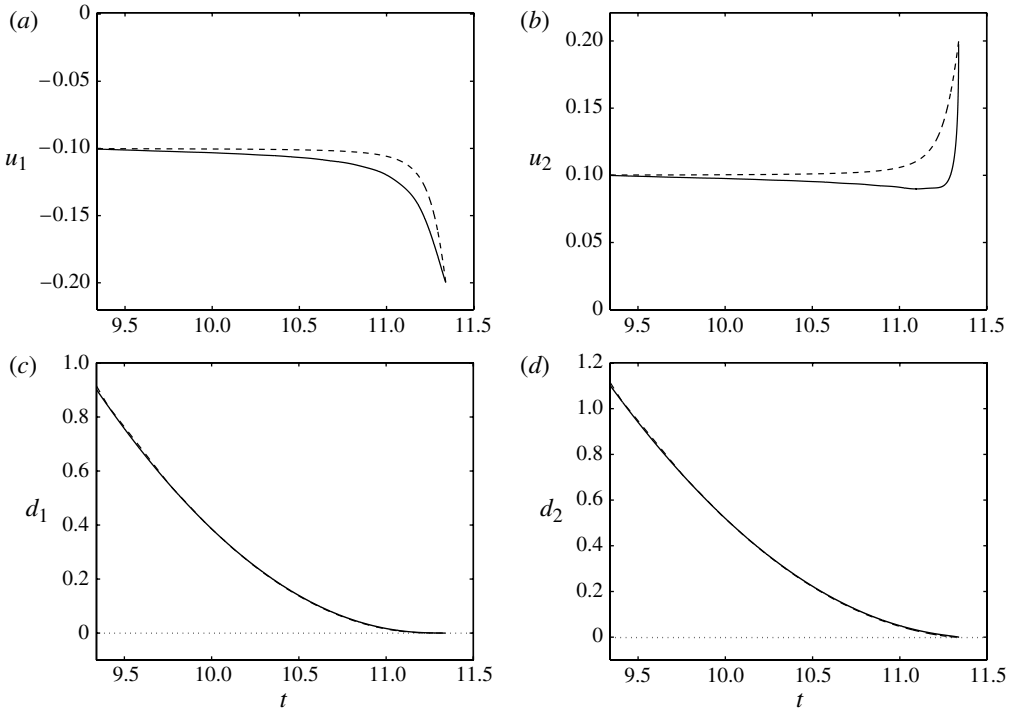


FIGURE 11. Comparison between the asymptotic solution in (5.10) (dashed lines) and the numerical solution (solid lines) for the 25th shock event of the periodic shock train with $\Delta\alpha = 0.4$.

and $\tau \in [0, 2]$. Further, it is

$$c_1 = 1 - \frac{\Delta\alpha}{4} - \frac{(\tau - \upsilon)}{2} \quad c_2 = 1 + \frac{\Delta\alpha}{4} - \frac{(\tau + \upsilon)}{2}. \tag{5.11}$$

All details of computations are reported in Appendix B. The asymptotic solution described in (5.10) predicts a shock wave which starts travelling inside the sloping region at $\tau = 0$ and reaches the shoreline at $\tau = 2$. The predicted velocity at the shoreline is $\upsilon = \Delta\alpha/2$ while at the seaward boundary (that is, for $\tau = 0$) $\upsilon \simeq \Delta\alpha/4$. Further, this is the value of the velocity field which is kept almost constant during the shock evolution (see, for example, the top left panel of figure 10).

In figure 11 the comparison between the asymptotic solution in (5.10) and the numerical solution is displayed for the 25th shock event of case (*b*) the train. The match is fairly good for the velocities and the largest discrepancies occur just seaward of the shoreline. However, the velocity profiles and the values at the seaward boundary and at the shoreline are well approximated. For what concerns the depth, the match is excellent for both d_1 and d_2 and the profiles of the numerical and asymptotic solutions are practically coincident.

The asymptotic solution in (5.10) may be useful not only for benchmarking wave-resolving models (such as, for example, the NSWEs or the numerous Boussinesq-type models) but also for wave-averaged models (e.g. SHORECIRC, SWAN, etc.). In fact, these models contains forcing terms which come from wave-resolving models and/or are obtained through approximated analytical solutions. In the latter case, such analytical solutions are generally derived through the linear theory of wave

https://doi.org/10.1017/jfm.2011.352 Published online by Cambridge University Press

propagation and, therefore, rely on a rough approximation and do not account for wave breaking. With respect to this, the asymptotic solution in (5.10) may be a useful benchmark for wave-averaged models.

6. Conclusions

On the basis of the work of Antuono (2010), a train of shock waves fed by a constant Riemann invariant has been built and studied in detail. The quasi-analytical solution proposed in the present work represents the first long-time solution for shock waves on planar beaches and, therefore, may have important implications in the evolution of both wave-resolving and wave-averaged models. To this purpose, the asymptotic behaviour of a train of such shock waves has been inspected providing useful relations/results for the mean water level set-up and for the mean dissipation induced by a single shock event. Finally, an approximate asymptotic solution for the shock wave propagation has been obtained. This solution, as well as the asymptotic relations for the mean quantities inside the sloping region, may be a useful benchmark for wave-averaged models.

The author would like to thank Professor Maurizio Brocchini for his useful comments and suggestions and Dr Luciano Soldini for the help received during the reviewing procedure.

Appendix A. Numerical details

Here, we prove that the correct root of polynomial (3.2) satisfies the following bounds:

$$\sqrt{c_1} \leqslant z \leqslant \frac{2(\Delta\alpha + c_1)}{\sqrt{c_1 + \sqrt{9c_1^2 + 8(\Delta\alpha)^2 + 16c_1\Delta\alpha}}}, \tag{A 1}$$

where the superscript (n) has been dropped for the ease of notation. First, let us define $\xi = s - u_1$ and rewrite (2.7) as follows:

$$d_2 = -\frac{d_1}{2} + \frac{1}{2}\sqrt{d_1^2 + 8d_1\xi^2} = \frac{4d_1\xi^2}{d_1 + \sqrt{d_1^2 + 8d_1\xi^2}}. \tag{A 2}$$

Since $z = c_2/\sqrt{c_1}$ and $\xi \geqslant 0$, using the equation above we immediately obtain

$$z = \frac{2\xi}{\sqrt{c_1 + \sqrt{c_1^2 + 8\xi^2}}}. \tag{A 3}$$

Now, rearranging the entropy conditions in (2.5), we find

$$c_1 \leqslant \xi \leqslant (u_2 - u_1) + c_2, \tag{A 4}$$

and, using the definition of α, we obtain

$$c_1 \leqslant \xi \leqslant \Delta\alpha - (c_2 - c_1) + c_1. \tag{A 5}$$

Since $(c_2 - c_1) \geqslant 0$, we overestimate the upper bound by writing

$$c_1 \leqslant \xi \leqslant \Delta\alpha + c_1. \tag{A 6}$$

Now, using (A 3), it is simple to prove that $\mathrm{d}z/\mathrm{d}\xi \geqslant 0$, this meaning that the expression in (A 3) is an increasing function of ξ. As a consequence, we substitute

https://doi.org/10.1017/jfm.2011.352 Published online by Cambridge University Press

the upper and lower bounds of (A 6) into (A 3) and obtain the upper and lower bounds in (A 1).

Appendix B. Asymptotic solution: details of derivation

In this section we derive the asymptotic solution for a periodic shock train. First, we prove that, for a shocks train starting from still water conditions, the following relation holds true for large n:

$$t_0^{(n)} = A^{(n)} - 2, \tag{B 1}$$

where $A^{(n)}$ has been defined in (5.2).

Proof. Let us consider the relation (3.3) and apply the following summation:

$$\sum_{2}^{n-1} \Delta t^{(k+1)} = 2 \sum_{2}^{n-1} \Delta\alpha^{(k)} - \sum_{2}^{n-1} \Delta t^{(k)}. \tag{B 2}$$

Since these series are telescopic, we simply obtain

$$t_0^{(n)} - t_0^{(2)} = 2(\alpha_2^{(n-1)} - \alpha_2^{(1)}) - (t_0^{(n-1)} - t_0^{(1)}). \tag{B 3}$$

According to the first formula in (3.3), $t_0^{(2)} = t_0^{(1)} + 2(\alpha_2^{(1)} - \alpha_2^{(0)})$ and, therefore, the expression above simplifies as follows:

$$t_0^{(n)} = -t_0^{(n-1)} + 2(\alpha_2^{(n-1)} - \alpha_2^{(0)}) + 2t^{(1)}. \tag{B 4}$$

Asymptotically, the shock events are periodic with period $T = \Delta\alpha$. As a consequence, for large values of n, we can assume $t_0^{(n-1)} \simeq t_0^{(n)} - \Delta\alpha$ and $\Delta\alpha \simeq \alpha_2^{(n)} - \alpha_2^{(n-1)}$. Substituting these relations into (B 4), we obtain

$$t_0^{(n)} = A^{(n)} - \alpha_2^{(0)} + t_0^{(1)}. \tag{B 5}$$

Since $\alpha_2^{(0)} = 2 + t_0^{(1)}$, the thesis is proved. □

Now, we are in a position to prove the asymptotic solution given in (5.10). Combining the expressions in (2.6), we obtain

$$u_2 - u_1 = (d_2 - d_1)\sqrt{\frac{d_2 + d_1}{2d_1 d_2}}, \tag{B 6}$$

that is,

$$\sqrt{2}c_1 c_2 (u_2 - u_1) = (c_2 - c_1)(c_2 + c_1)\sqrt{c_2^2 + c_1^2}. \tag{B 7}$$

Let us assume $u_2 = -u_1 = \upsilon$ so that $u_2 + u_1 \equiv 0$ and define $\tau = t - t_0^{(n)}$ where $t_0^{(n)}$ is given by (B 1). Since $c = (\alpha - \upsilon - t)/2$, it follows that

$$c_1 = 1 - \frac{\Delta\alpha}{4} - \frac{(\tau - \upsilon)}{2} \qquad c_2 = 1 + \frac{\Delta\alpha}{4} - \frac{(\tau + \upsilon)}{2}. \tag{B 8}$$

At the shoreline $c_1 = c_2 = 0$ and the expressions above imply $\upsilon = \Delta\alpha/2$ at $\tau = 2$. Substituting these expressions in (B 7) and rearranging, we find

$$\upsilon\left[(2-\tau)^2 - \left(\frac{\Delta\alpha}{2} - \upsilon\right)^2\right] = (2-\tau)\left(\frac{\Delta\alpha}{2} - \upsilon\right)\sqrt{(2-\tau)^2 + \left(\frac{\Delta\alpha}{2} - \upsilon\right)^2} \tag{B 9}$$

https://doi.org/10.1017/jfm.2011.352 Published online by Cambridge University Press

Now, using

$$\xi = \frac{2-\tau}{\Delta\alpha/2-\upsilon}, \tag{B 10}$$

we obtain

$$\xi^2 - 1 = \left(\frac{\Delta\alpha}{2\upsilon} - 1\right)\xi\sqrt{\xi^2+1}, \tag{B 11}$$

or simply

$$\xi^2 - 1 = \kappa\xi\sqrt{\xi^2+1}, \tag{B 12}$$

where $\kappa = \Delta\alpha/(2\upsilon) - 1$. On the basis of the observation of the numerical solutions, κ and ξ are assumed to be positive and finite. Then, squaring and solving, we find two possible solutions:

$$\xi = \left(\frac{2+\kappa^2 \pm \kappa\sqrt{\kappa^2+8}}{2(1-\kappa^2)}\right)^{1/2}. \tag{B 13}$$

Comparing them with the numerical outputs, one finds that the correct solution is that with the positive sign. Using (B 10), this can be rewritten as follows:

$$2-\tau = \frac{\Delta\alpha}{2}\frac{\kappa}{\kappa+1}\left(\frac{2+\kappa^2+\kappa\sqrt{\kappa^2+8}}{2(1-\kappa^2)}\right)^{1/2}. \tag{B 14}$$

This expression is singular for $\kappa = 1$, that is, for $\upsilon = \Delta\alpha/4$ implying that this value is achieved for $\tau \to -\infty$. Anyway, an approximate solution at the seaward boundary (that is, at $\tau = 0$) can be obtained by expanding the right-hand side of (B 14) in the neighbourhood of $k = 1$ (or, equivalently, assuming $k = 1-\varepsilon$ with $0 < \varepsilon \ll 1$). We obtain

$$\kappa|_{\tau=0} = 1 - \frac{36\Delta\alpha^2}{25\Delta\alpha^2 + 768 + 16\sqrt{6}\sqrt{25\Delta\alpha^2+384}} + O(\Delta\alpha^4). \tag{B 15}$$

Since the last term on the right-hand side is, generally, small, the approximate solution predicts $\kappa \simeq 1$ (that is, $\upsilon \simeq \Delta\alpha/4$) at $\tau = 0$ as observed in the numerical solutions.

Appendix C. The energy equation and the integral NSWEs

The energy equation for the NSWEs is obtained by combining the continuity and momentum equations. This means that in the framework of the NSWEs the total energy is not an independent quantity but depends on both depth and volume flux.

First, let us rewrite the momentum equation in the following non-conservative form:

$$u_t + uu_x + d_x = h_x. \tag{C 1}$$

Then, multiplying it by u, we obtain the kinetic energy equation:

$$\left(\frac{u^2}{2}\right)_t + u\left(\frac{u^2}{2}\right)_x + ud_x = uh_x. \tag{C 2}$$

Now, adding the continuity equation, we find

$$\left(\frac{u^2}{2}+d\right)_t + u\left(\frac{u^2}{2}+d\right)_x + (ud)_x = uh_x, \tag{C 3}$$

https://doi.org/10.1017/jfm.2011.352 Published online by Cambridge University Press

or equivalently

$$\left(\frac{u^2}{2}+d\right)_t + u\left(\frac{u^2}{2}+d\right)_x - d_t = uh_x. \tag{C 4}$$

The quantity $(u^2/2+d)$ represents the total energy (kinetic plus potential) per unit of mass. To get the conservative format of (C 4), it is sufficient to multiply it for the water depth and rearrange the derivatives as follows:

$$\left[d\left(\frac{u^2}{2}+d\right)\right]_t + \left[u\,\mathrm{d}\left(\frac{u^2}{2}+d\right)\right]_x - [d_t+(ud)_x]\left(\frac{u^2}{2}+d\right) - dd_t = u\,\mathrm{d}h_x. \tag{C 5}$$

Finally, using the continuity equation, we find

$$\left[d\left(\frac{u^2}{2}+\frac{d}{2}\right)\right]_t + \left[u\,\mathrm{d}\left(\frac{u^2}{2}+d\right)\right]_x = u\,\mathrm{d}h_x, \tag{C 6}$$

or, equivalently,

$$\left(\frac{Q^2}{2d}+\frac{d^2}{2}\right)_t + \left(\frac{Q^3}{2d^2}+dQ\right)_x = Qh_x. \tag{C 7}$$

The forcing term on the right-hand side can be moved inside the fluxes. In fact, using the continuity equation and the fact that $h=h(x)$, we can write

$$Qh_x = (Qh)_x - Q_x h = (Qh)_x + d_t h = (Qh)_x + (dh)_t. \tag{C 8}$$

As a consequence, (C 7) becomes

$$\left(\frac{Q^2}{2d}-\frac{d^2}{2}+\eta d\right)_t + \left(\frac{Q^3}{2d^2}+\eta Q\right)_x = 0, \tag{C 9}$$

or, equivalently,

$$\left(\frac{Q^2}{2d}+\frac{\eta^2}{2}\right)_t + \left(\frac{Q^3}{2d^2}+\eta Q\right)_x = 0. \tag{C 10}$$

Now, let us integrate (C 10) for $x\in[-1,x_N(t)]$ and $h(x)=-x$. Since the fluid domain is cut by shock waves, the integration has to be done by collecting together the spatial intervals in which the solution is continuous. Then, using the Leibniz rule and the conditions $d=Q=0$ and $\eta=x_N(t)$ at $x=x_N(t)$, we, finally, obtain

$$\dot{E} - \frac{x_N^2\dot{x}_N}{2} - \left(\frac{Q_0^3}{2d_0^2}+\eta_0 Q_0\right) + \sum_{k=1}^{n}\left\{-s^{(k)}\left[\left[\frac{Q^2}{2d}+\frac{\eta^2}{2}\right]\right]^{(k)} + \left[\left[\frac{Q^3}{2d^2}+\eta Q\right]\right]^{(k)}\right\} = 0, \tag{C 11}$$

where the subscript 0 indicates quantities at the seaward boundary ($x=-1$), n represents the number of shock waves which are inside the fluid domain at the time t and

$$E(t) = \int_{-1}^{x_N(t)}\left(\frac{Q^2}{2d}+\frac{\eta^2}{2}\right)\mathrm{d}x. \tag{C 12}$$

As explained in Stoker (1957), the jump relations for the energy equation do not close to zero and represent the dissipation induced by the shock waves. This implies that each term of the summation in (C 11) is positive. In contrast, when this procedure is

https://doi.org/10.1017/jfm.2011.352 Published online by Cambridge University Press

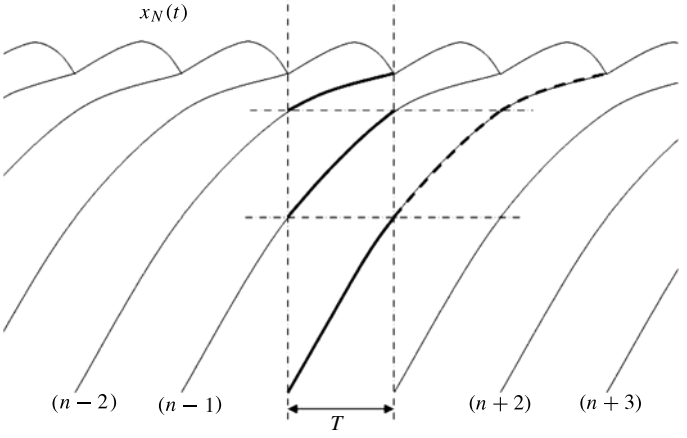


FIGURE 12. Sketch of the integration over a wave period for the periodic shock train. The thick solid lines indicate the intervals of different shock waves which appear inside a wave period. The thick dashed lines indicate their rearrangement into a single shock event.

applied to the continuity and momentum equations, these terms are all identically null and give the shock relations in (2.4).

Applying the time-average operator to (C 11) along with the periodicity of the solution and the continuity of $x_N(t)$, it immediately follows:

$$\langle \mathscr{D} \rangle = \left\langle \left[\frac{Q_0^3}{2d_0^2} + \eta_0 Q_0 \right] \right\rangle, \tag{C 13}$$

where $\langle \mathscr{D} \rangle$ represents the average of the dissipation induced by the shock waves. It is easy to convince oneself, that, under the hypothesis that the solution is periodic, $\langle \mathscr{D} \rangle$ coincides with the mean of the dissipation induced by a *single* shock event (see, for example, figure 12). Applying the same procedure shown above to the continuity and the momentum equations, we find

$$\langle Q_0 \rangle = 0, \quad \langle V \rangle = \left\langle \left[\frac{d_0^2}{2} + \frac{Q_0^2}{d_0} \right] \right\rangle \quad \text{with } V(t) = \int_{-1}^{x_N(t)} d(t, x)\, \mathrm{d}x. \tag{C 14}$$

Finally, let us consider again (C 11). After some lengthy algebra, it is possible to rearrange the (local) dissipative terms as follows:

$$-s \left[\left[\frac{Q^2}{2d} + \frac{\eta^2}{2} \right] \right] + \left[\left[\frac{Q^3}{2d^2} + \eta Q \right] \right] = -\frac{m}{4d_1 d_2} [\![d]\!]^3, \tag{C 15}$$

where $m = (u_2 - s)d_2 = (u_1 - s)d_1$ is the mass flux across the shock wave. For a shock wave generated by the collapse of the α characteristic curves, $m \leqslant 0$ while $[\![d]\!] \geqslant 0$ and, therefore, the expression in (C 15) is positive as expected. This term, first found by Stoker (1957), relates the dissipation to the mass flux across the shock wave and to the jump of the water depth.

REFERENCES

ANTUONO, M. 2010 A shock solution for the nonlinear shallow water equations. *J. Fluid Mech.* **658**, 166–187.

ANTUONO, M. & HOGG, A. J. 2009 Run-up and backwash bore formation from dam-break flow on an inclined plane. *J. Fluid Mech.* **640**, 151–164.

https://doi.org/10.1017/jfm.2011.352 Published online by Cambridge University Press

ANTUONO, M., HOGG, A. J. & BROCCHINI, M. 2009 The early stages of a shallow flow in an inclined flume. *J. Fluid Mech.* **633**, 285–309.

ANTUONO, M. & BROCCHINI, M. 2007 The boundary value problem for the nonlinear Shallow Water equations. *Stud. Appl. Maths* **119**, 73–93.

ABREU, T., SILVA, P. A., SANCHO, F. & TEMPERVILLE, A. 2010 Analytical approximate wave form for asymmetric waves. *Coast. Engng* **57**, 656–667.

BOOIJ, N., RIS, R. C. & HOLTHUIJSEN, L. H. 1999 A third-generation wave model for coastal regions. 1. Model description and validation. *J. Geophys. Res.* **104**, 7649–7666.

BRIGANTI, R., MUSUMECI, R. E., BELLOTTI, G., BROCCHINI, M. & FOTI, E. 2004 Boussinesq modelling of breaking waves: description of turbulence. *J. Geophys. Res.* **109** (C7), 7015 doi:10.1029/2003JC002065.

BROCCHINI, M. & DODD, N. 2008 Nonlinear shallow water equations modelling for coastal engineering. *J. Waterway Port Coast. Ocean Engng* **134**, 104–120.

BROCCHINI, M., KENNEDY, A., SOLDINI, L. & MANCINELLI, A. 2004 Topographically-controlled, breaking wave-induced macrovortices. Part 1. Widely separated breakwaters. *J. Fluid Mech.* **507**, 289–307.

BROCCHINI, M., BERNETTI, R., MANCINELLI, A. & ALBERTINI, G. 2001 An efficient solver for nearshore flows based on the WAF method. *Coast. Engng* **43** (2), 105–129.

BROCCHINI, M. & PEREGRINE, D. H. 1996 Integral flow properties of the swash zone and averaging. *J. Fluid Mech.* **317**, 241–273.

DRAKE, T. G. & CALANTONI, J. 2001 Discrete particle model for sheet flow sediment transport in the nearshore. *J. Geophys. Res.* **106** (C9), 19859–19868.

ELFRINK, B. & BALDOCK, T. E. 2002 Hydrodynamics and sediment transport in the swash zone: a review and perspectives. *Coast. Engng* **45**, 149–167.

ELGAR, S. & GUZA, R. T. 1985 Observations of bispectra of shoaling surface gravity waves. *J. Fluid Mech.* **161**, 425–448.

GUARD, P. A. & BALDOCK, T. E. 2007 The influence of seaward boundary conditions on swash zone hydrodynamics. *Coast. Engng* **54**, 321–331.

HOGG, A. J., BALDOCK, T. E. & PRITCHARD, D. 2011 Overtopping a truncated planar beach. *J. Fluid Mech.* **666**, 521–553.

HUBBARD, M. E. & DODD, N. 2002 A 2D numerical model of wave run-up, overtopping and regeneration. *Coast. Engng* **47** (1), 1–126.

JEFFREY, A. 1976 *Quasilinear Hyperbolic Systems and Waves*. Pitman.

KAIHATU, J. M., VEERAMONY, J., EDWARDS, K. L. & KIRBY, J. T. 2007 Asymptotic behaviour of frequency and wavenumber spectra of nearshore shoaling and breaking waves. *J. Geophys. Res.* **112** (C6), C06016.

KENNEDY, A. B., CHEN, Q., KIRBY, J. T. & DARLYMPLE, R. A. 2000 Boussinesq modelling of wave transformation, breaking and run-up. I: one dimension. *J. Waterway Port Coast. Ocean Engng* **126**, 39–47.

KENNEDY, A., BROCCHINI, M., SOLDINI, L. & GUTIERREZ, E. 2006 Topographically-controlled, breaking wave-induced macrovortices. Part 2. Changing geometries. *J. Fluid Mech.* **559**, 57–80.

LAX, P. D. 1957 Hyperbolic systems of conservation laws II. *Commun. Pure Appl. Math.* **10**, 537–566.

LEVEQUE, R. 2002 *Finite Volume Methods for Hyperbolic Problems*. Cambridge University Press.

PARK, K. Y. & BORTHWICH, A. G. L. 2001 Quadtree grid numerical model of nearshore wave-current interaction. *Coast. Engng* **42** (3), 219–239.

PRITCHARD, D. & HOGG, A. J. 2005 On the transport of suspended sediment by a swash event on a plane beach. *Coast. Engng* **52**, 1–23.

RYRIE, S. C. 1983 Longshore motion generated on beaches by obliquely incident bores. *J. Fluid Mech.* **129**, 193–212.

SHEN, M. C. & MEYER, R. E. 1963 Climb of a bore on a beach. Part 3. Run-up. *J. Fluid Mech.* **16**, 113–125.

STOKER, J. J. 1957 *Water Waves*. Interscience Publishers, Inc.

https://doi.org/10.1017/jfm.2011.352 Published online by Cambridge University Press

SUNTOYO, , TANAKA, H. & SANA, A. 2008 Characteristics of turbulent boundary layers over a rough bed under saw-tooth waves and its application to sediment transport. *Coast. Engng* **55** (12), 1102–1102.

SVENDSEN, I. A. 1994 Wave heights and set-up in a surf zone. *Coast. Engng* **8** (4), 303–329.

TING, F. C. K. & KIRBY, J. T. 1994 Observation of undertow and turbulence in a laboratory surf zone. *Coast. Engng* **24** (1–2), 51–80.

TORO, E. F. 2001 *Shock Capturing Methods for Free-Surface Shallow Flows*. John Wiley and Sons.

VAN DONGEREN, A. R., SANCHO, F. E., SVENDSEN, I. A. & PETREVU, U. 1994 SHORECIRC: a quasi 3D nearshore model. In *Proceedings of the 24th International Conference on Coastal Engineering*, pp. 2741–2754. ASCE.

WHITHAM, G. B. 1974 *Linear and Nonlinear Waves*. Wiley.

ZHANG, Q. & LIU, P. L.-F. 2008 A numerical study of swash flows generated by bores. *Coast. Engng* **55**, 1113–1134.

https://doi.org/10.1017/jfm.2011.352 Published online by Cambridge University Press